

# Training Feedforward Neural Networks with Standard Logistic Activations is Feasible

Emanuele Sansone, and Francesco G.D. De Natale, *Member, IEEE*

**Abstract**—Training feedforward neural networks with standard logistic activations is considered difficult because of the intrinsic properties of these sigmoidal functions. This work aims at showing that these networks can be trained to achieve generalization performance comparable to those based on hyperbolic tangent activations. The solution consists on applying a set of conditions in parameter initialization, which have been derived from the study of the properties of a single neuron from an information-theoretic perspective. The proposed initialization is validated through an extensive experimental analysis.

**Index Terms**—Deep Neural Networks, Recurrent Neural Networks, Sigmoid Activations, Initialization



## 1 INTRODUCTION

DEEP LEARNING has received a lot of attention in the last decade due to the impressive performance achieved in numerous computer vision tasks, including object detection [1], human action recognition [2], image restoration [3] and image classification [4], and in natural language tasks, including language modelling [5], parsing [6], machine translation [7] and speech-to-text translation [8]. The success of deep learning is due to the capability of transforming input data into representations that are increasingly more abstract with depth and in a way that resembles the brain structure of primates [9]. Recent theoretical analysis provides partial confirmation on the experimental findings obtained by deep learning models and show that there is an exponential advantage in terms of the complexity of functions computed by deep architectures over shallow ones [10], [11], [12].<sup>1</sup>

Deep learning models are impactful in many real-world applications, and the transfer of this technology to society has created new emerging issues, like the need of model interpretability [14]. The General Data Protection Regulation approved in 2016 by the European parliament, which will be effective in 2018, is a concrete example of the need to provide human understandable justifications for decisions taken by automated data-processing systems [15].

Research could probably be inspired by old literature in neural networks to find better explanations about the dynamics of deep learning and provide more human interpretable solutions. An example of such process is found in standard logistic activation functions, that have been studied extensively in the past, but tend to be substituted by other activation functions in modern neural networks. To understand why this may be the case, it is important to recall the unique properties of the logistic function and therefore analyze the reasons why it has been introduced in neural networks. Firstly, the standard logistic function is biologically plausible. In fact, it is one of the best differentiable approximations to the leaky integrate-and-fire model, used

in neuroscience to model the spiking behaviour of biological neurons [16]. Biological plausibility can be essential for driving deep learning research towards the uncovering of human learning dynamics and also providing explanations that are effectively interpreted by humans [17]. Secondly, there is theoretical work showing that a family of neural networks provided with standard logistic activations can be equivalently converted into fuzzy rule-based systems [18], thus raising the possibility to perform reasoning using fuzzy logic and potentially extract human interpretable explanations of predictions made by deep learning models [19].

While the standard logistic function is used extensively as activation in shallow neural networks, it receives less attention in deep learning. A common justification supporting this fact is that training these deep neural networks is very challenging due to the intrinsic properties of the standard logistic function, like its non-zero mean output value [20], [21] and its low derivative score in zero [22]. The bounded alternative to the standard logistic activation is the hyperbolic tangent, which allows an easier training. Nevertheless, this function is not biologically plausible and does not have any relation with fuzzy logic. This work aims at showing that training deep feedforward neural networks with standard logistic activations can be feasible through careful initialization. In particular, we derive some conditions using information theory that are used as principled criteria for initialization. We show through extensive experimental analysis that our conditions guarantee a better propagation of information through the whole network and that during training no vanishing gradients are observed, thus boosting the convergence speed of the optimizer. The proposed initialization outperforms the other existing strategies also in terms of generalization performance and contribute to bridge the gap between networks with standard logistic activations and networks with hyperbolic tangents.

The rest of the paper is organized as follows. Section 3 provides a preliminary discussion on the statistical properties of a single neuron with standard logistic activation function. Section 4 studies the neuron from an information-theoretic perspective and derives initialization conditions for its parameters. Section 5 relates the proposed conditions

1. We refer to shallow models to indicate networks with a single hidden layer, while we refer to deep models for networks with more than one hidden layer [13].

with the problem of vanishing gradients. Finally, Section 6 validates the theory over different well-known benchmarks and different networks.

## 2 LITERATURE REVIEW

In 1986, Rumelhart et al. [23] propose the backpropagation algorithm to train a feedforward neural network.<sup>2</sup> In this seminal work, the authors use random weight initialization to break the symmetry of parameters and allow to perform credit assignment during training, namely knowing how to compute each weight contribution to the final error. Nevertheless, the initial choice of parameters plays an important role on determining the generalization performance of the final trained network, as it is demonstrated by subsequent works (see [25] for an empirical comparison among the main works of the period until 2000 and [26] for an updated summary of the related work up to 2004). In that period, the research about initialization focused mainly on shallow architectures, motivated by the fact that (i) shallow neural networks are universal function approximators [27], [28] and (ii) deep networks are more difficult to train than shallow counterparts [29], due to the problem of vanishing and exploding gradients. Authors in [20] are probably among the few to propose initialization strategies for deep learning. In particular, they use random weight initialization in combination with hand-crafted activations for hidden neurons. We will see in the experimental section that their proposed initialization strategy is not particularly suited for standard logistic activations, as it is strongly affected by vanishing/ exploding gradients.

The first effective strategy to learn deep models appears in 2006 [30] and consists of splitting the learning process into two stages, called unsupervised pre-training and fine-tuning, respectively. In the first stage, an unsupervised algorithm is applied layerwise to learn increasingly more complex representations of the input features.<sup>3</sup> In the second stage, network parameters are updated/fine-tuned using a supervised criterion and gradient-based optimization. An explanation for this success appears later in [33], where the authors show experimentally that unsupervised pre-training can be regarded as an effective initialization strategy for the subsequent optimization stage. In other words, "pre-training guides the learning towards basins of attraction of minima that support better generalization from the training data set" [33].

Unsupervised pre-training is extremely expensive from a computational perspective and alternatives are proposed to overcome the problem of vanishing/exploding gradients. In particular, there are solutions, which modify the structure of neural networks with skip connections between hidden layers [34], [35], [36] or with new normalizing layers [37], [38], [39], in order to guarantee the continuous flow of information through the network. Other approaches study the properties of the loss surface and develop training algorithms able to find better minima. In particular, we find

2. Even if, the author in [24] argues that backpropagation is dated back to the early 1960s.

3. Authors in [30] use Restricted Boltzmann machines at each layer to learn deep belief nets, while authors in [31], [32] use stacked autoencoders to learn deterministic networks.

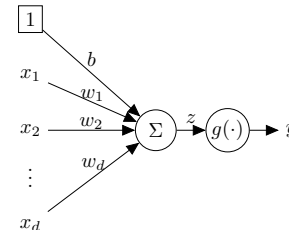


Fig. 1. Graphical visualization of a single neuron.

(i) optimization algorithms based on accelerated gradients, like momentum [40], [41] and Adam [42], which combine information about past and current gradients in order to dampen the oscillations on the loss surface observed during training, thus converging faster to the final solution, and (ii) second-order optimization strategies, like Hessian-free [43] and natural gradient methods [44], [45], which looks for efficient approximations of the Hessian using the Gauss-Newton [46] and the Fisher information matrices, respectively. There are a plethora of works studying optimization in neural networks, therefore we invite the interested reader to see the recent work in [47], which provides a theoretical comparative analysis between different accelerated gradient-based algorithms, and the survey in [48], which presents a more general overview of optimization strategies in machine learning.

One of the most influential studies about initialization in the last decade is the work of [21]. In particular, the authors observes that "the logistic sigmoid activation is unsuited for deep networks with random initialization because of its mean value, which can drive especially the top hidden layer into saturation". Other more recent works, see for example [22], confirm the fact that the standard logistic activation is more difficult to train than other activations and proper rescaling, making the logistic function similar to the hyperbolic tangent, is required for successful training. Alternative activations are therefore proposed in the literature. The rectifier linear function is one of the most appealing solutions [49],<sup>4</sup> because of its unbounded nature that allow the gradient not to vanish. Principled criteria based on orthogonality [51] and normalization of weights [52] are used in combination with random weight initialization to find better starting solutions for training these networks.

Recent theoretical analysis on the properties of random initialization, see [53] for the analysis of rectifier linear functions and [54] for a more general theory validated also on hyperbolic tangents, reveals that there exists a range of values for the variance of weights which are more suited for the propagation of gradients, thus improving the trainability of networks. Our work proposes to study the more difficult problem of training standard logistic activations from the initialization perspective. Furthermore, we shed light on a more general criterion to derive initializing conditions, that explicitly maximizes the amount of information propa-

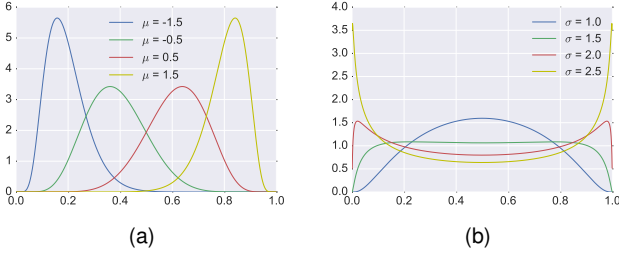


Fig. 2. Visualization of density  $p_y(y)$  for different settings of  $\mu, \sigma$ . (a)  $\sigma = 0.5$  and variable  $\mu$ , (b)  $\mu = 0$  and variable  $\sigma$ .

gation in neural networks.

### 3 STATISTICAL BACKGROUND

Let us recall the statistical properties of a single neuron characterized by an input vector  $\mathbf{x} \in \mathbb{R}^d$ , a weight vector  $\mathbf{w} \in \mathbb{R}^d$ , a bias  $b \in \mathbb{R}$  and a standard logistic activation function  $g(z) = 1/(1 + e^{-z})$ . Fig. 1 provides a graphical interpretation of the computational unit used in many neural networks.

Consider  $z$  as the logit of the given neuron, namely  $z = \sum_{i=1}^d w_i x_i + b = \mathbf{w}^T \mathbf{x} + b$ . By modelling the inputs as independent random variables, with densities/distributions characterized by finite means and finite variances, it is possible to exploit the Lyapunov theorem<sup>5</sup> and model  $z$  as a Gaussian random variable with mean  $\mu$  and variance  $\sigma^2$ . In this case,  $\mu = \sum_{i=1}^d w_i E\{x_i\} + b$  and  $\sigma^2 = \sum_{i=1}^d w_i^2 Var\{x_i\}$ , where  $E\{\cdot\}$  and  $Var\{\cdot\}$  are the expected value and the variance operators, respectively. It is interesting to note that the mean value of the Gaussian density associated with  $z$  is mainly dominated by the parameter  $b$  (especially when  $E\{x_i\} = 0, \forall i = 1, \dots, d$ , since  $\mu = b$ ), while its variance is influenced only by the weight vector  $\mathbf{w}$ . Therefore, all subsequent considerations valid for  $\mu$  and  $\sigma$  will be valid also for  $b$  and  $\mathbf{w}$ , respectively.

Due to its nonlinearity, the activation function  $g(z)$  produces an output with different statistical properties from the ones associated with logit  $z$ . In fact, the density associated with output  $y \in (0, 1)$  can be expressed by the following relation, namely:

$$p_y(y) = \frac{1}{y(1-y)\sqrt{2\pi\sigma^2}} \exp\left\{-\frac{(\ln \frac{y}{1-y} - \mu)^2}{2\sigma^2}\right\} \quad (1)$$

which is not any more a Gaussian density, as can be seen from Fig. 2. It is important to mention that  $\mu$  and  $\sigma$  controls the mean and variance of  $p_y(y)$ , and therefore also the amount of information that can be propagated through the neuron. In fact, for very large or very small values of  $\mu$ , we have no information propagation, since the activation function is saturated and the output variance tends to zero (see Fig. 2(a)). The same happens for small values of  $\sigma$ , because in this case  $p_y(y)$  behaves similarly to a Dirac delta centered at  $g(\mu)$ . It can be shown that, when  $\sigma \rightarrow \infty$ , the

4. Many different extensions are also proposed. For example, [50] parameterize the rectifier linear function to allow non-zero gradient in the negative region.

5. This is an extension of the central limit theorem, which relaxes the assumptions over the random variables and require that the random variables are independent but not necessarily identically distributed.

density  $p_y(y)$  approaches a Bernoulli distribution.<sup>6</sup> This is an extreme case, where information can be propagated, but the output becomes discrete (see Fig. 2(b)).

In the next section, the behaviour of the neuron is analyzed more in detail from the perspective of information theory.

### 4 INFORMATION-THEORETIC ANALYSIS

In this section, we ask the following question: which region of the parameter space  $(\mu, \sigma)$  guarantees that the maximum amount of information is propagated through the activation function  $g(z)$ ? We address this question by formulating the problem as an optimization.

Logit  $z$  and output  $y$  are modelled as continuous random variables distributed according to  $\mathcal{N}(\mu, \sigma^2)$  and  $p_y(y)$ , respectively. We choose the entropy of  $y$ , viz.  $H(y)$ , as the objective of the maximization problem and discard for example the mutual information, since it is not defined for this particular case.<sup>7</sup> Therefore, the objective can be written in the following way:

$$\begin{aligned} H(y) &\doteq - \int_0^1 p_y(y) \ln p_y(y) dy \\ &= \int_{-\infty}^{\infty} \frac{e^{-\frac{(z-\mu)^2}{2\sigma^2}}}{\sqrt{2\pi\sigma^2}} \left\{ \frac{(z-\mu)^2}{2\sigma^2} + \right. \\ &\quad \left. + \ln [g(z)(1-g(z))\sqrt{2\pi\sigma^2}] \right\} dz \\ &= \int_{-\infty}^{\infty} \frac{e^{-\frac{(z-\mu)^2}{2\sigma^2}}}{\sqrt{2\pi\sigma^2}} \left\{ \frac{(z-\mu)^2}{2\sigma^2} + \ln \sqrt{2\pi\sigma^2} + \ln g'(z) \right\} dz \\ &= H(z) + E_z\{\ln g'(z)\} \end{aligned} \quad (2)$$

where  $H(z)$ ,  $E_z\{\cdot\}$ ,  $g'(z)$  are the entropy, the expected value and the derivative of  $g(\cdot)$  computed on variable  $z$ , respectively. Note that the second line in (2) is obtained from the first one by a simple change of variable, namely  $y = g(z)$ . Thus, the information coming out from the neuron is proportional to the information of the logit and the shape of the activation function.

In general, the term  $E_z\{\ln g'(z)\}$  in (2) is difficult to compute analytically and can be approximated using a lower and an upper bound (see Appendix A). This brings us to the following inequalities:

$$H_B(\mu, \sigma) - 2 \ln 2 \leq H(y) < H_B(\mu, \sigma) \quad (3)$$

and

$$\begin{aligned} H_B(\mu, \sigma) &\doteq \frac{1}{2} + \frac{1}{2} \ln(2\pi\sigma^2) - \\ &\quad - \mu \operatorname{erf}\left(\frac{\mu}{\sigma\sqrt{2}}\right) - \frac{2\sigma}{\sqrt{2\pi}} e^{-\frac{\mu^2}{2\sigma^2}} \end{aligned} \quad (4)$$

where  $\operatorname{erf}(\cdot)$  is the error function [55] and the function  $H_B(\mu, \sigma)$  can be visualized in Fig. 3. From 3,  $H_B(\mu, \sigma)$  defines both the lower and upper bounds of  $H(y)$ . Therefore, it can be used as a surrogate objective for our maximization

6.  $p_y(y) \rightarrow 0$  on the interval  $(0, 1)$  and the mass fully concentrates on the extrema of the interval.

7. It is not defined because of Dirac delta distributions, which come from the fact that  $g(\cdot)$  is deterministic and that the variables are continuous.

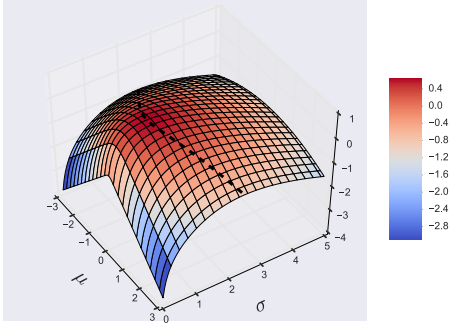


Fig. 3. 3D plot of  $H_B(\mu, \sigma)$ . The dotted curve on the surface represents the set of points for which  $\frac{\partial H_B(\mu, \sigma)}{\partial \sigma} = 0$ .

problem to find the optimal values of  $\mu$  and  $\sigma$ . Based on this principle, we can enunciate the following theorem (proof in Appendix B).

**Theorem 1.** The optimality conditions for  $H_B(\mu, \sigma)$ , defined in (4), are given by the following statements:

- $\forall \sigma \in \mathbb{R}^+, \frac{\partial H_B(\mu, \sigma)}{\partial \mu} = 0 \Rightarrow \mu = 0,$
- $\forall \mu \in \mathbb{R}, \frac{\partial H_B(\mu, \sigma)}{\partial \sigma} = 0 \Rightarrow \sigma = \sqrt{\frac{\pi}{2}} e^{\frac{W\left(\frac{2\mu^2}{\pi}\right)}{2}},$

where  $W(\cdot)$  is the principal branch of the Lambert W function [56]. The optimal solution, maximizing  $H_B(\mu, \sigma)$ , is therefore obtained at the point  $\mu = 0$  and  $\sigma = \sqrt{\frac{\pi}{2}} \approx 1.2533$ .

The optimality result given by Theorem 1 is interpreted as a condition on  $\mu$  and  $\sigma$  to have maximum amount of information propagated through the sigmoid activation. On one hand, the condition  $\mu = 0$  implies that  $b = -\sum_{i=1}^d w_i E\{x_i\}$  (following directly from Section 3), meaning that the expected value associated with the logit  $z$  must lie in the central part of the sigmoid far away from its saturating regions. On the other hand, the condition  $\sigma = \sqrt{\pi/2}$  for  $\mu = 0$  implies that  $\sum_{i=1}^d w_i^2 \text{Var}\{x_i\} = \pi/2$  (following directly from Section 3). Note that, if the variances of inputs are equal to the same constant, namely  $\text{Var}\{x_i\} = k$  for all  $i = 1, \dots, d$ ,<sup>8</sup> then  $\|\mathbf{w}\|_2 = \sqrt{\pi/(2k)}$ . This means that the maximum amount of information propagated through  $g(z)$  is obtained when vector  $\mathbf{w}$  lies on the hypersphere of radius  $\sqrt{\pi/(2k)}$ . In Appendix C, we show how to deal with the more general case where the input variances are different from each other. In practice, condition  $\sum_{i=1}^d w_i^2 \text{Var}\{x_i\} = \pi/2$  may be rewritten as  $\mathbf{w}^T \mathbf{D} \mathbf{w} = \pi/2$ , where  $\mathbf{D} \doteq \text{diag}\{\text{Var}\{x_1\}, \dots, \text{Var}\{x_d\}\}$ . If  $\mathbf{D}$  is positive definite, then the quadratic equation  $\mathbf{w}^T \mathbf{D} \mathbf{w} = \pi/2$  characterizes a multidimensional ellipsoid. Vector  $\mathbf{w}$  must therefore lie on this geometric locus of points to guarantee the maximal information propagation.

We argue that the obtained results are useful to define the initial conditions for learning the parameters of neurons with standard logistic activations and that cannot be enforced during training, because they limit the expressivity of the neural network. In fact, they impose that each neuron

lies in the linear region of its sigmoid activation, thus constraining the whole network to approximate only a linear function.

In the next sections, we provide theoretical evidence about the utility of these conditions.

## 5 THE PROBLEM OF VANISHING GRADIENTS

In this section, we study the implications of maximizing the mutual information at each neuron on the problem of vanishing gradients [29], [58]. In particular, we will show that the conditions established by Theorem 1 ensure that the selected starting point lies far away from the critical point that implies the occurrence of the vanishing gradients. Although the proposed theoretical analysis does not imply that this condition cannot be reached at some later stage of the learning, the effectiveness of the proposed initialization will be also supported by the extensive testing, presented in the experimental section.

We study the problem of vanishing gradients by adopting the same methodological analysis of [29], [58] and focus on recurrent neural networks, which can be seen as the deepest version of feedforward neural nets. The obtained results are therefore valid for traditional feedforward neural networks [29], [58].

Recall that a recurrent neural network is fully described by the following equations:

$$\begin{aligned} \mathcal{E}^t &= g(\mathbf{W}_{out} \mathbf{y}^t + \mathbf{b}_{out}) \\ \mathbf{y}^t &= g(\mathbf{W} \mathbf{y}^{t-1} + \mathbf{W}_{in} \mathbf{x}^t + \mathbf{b}) \end{aligned} \quad (5)$$

where  $t$  is used to identify time, or equivalently to indicate the layer in a deep feedforward neural net.  $\mathbf{x}^t \in \mathbb{R}^d$ ,  $\mathbf{y}^t \in \mathbb{R}^h$  and  $\mathcal{E}^t \in \mathbb{R}^o$  are the input, the hidden state and the output vectors of the network, respectively.  $\mathbf{W}_{in} \in \mathbb{R}^{h \times d}$ ,  $\mathbf{W} \in \mathbb{R}^{h \times h}$  and  $\mathbf{W}_{out} \in \mathbb{R}^{o \times h}$  are the weight matrices associated with the connections of neurons,  $\mathbf{b} \in \mathbb{R}^h$  and  $\mathbf{b}_{out} \in \mathbb{R}^o$  are the bias vectors and  $g(\cdot)$  is an element-wise operator that applies the sigmoid function to the incoming vector.

Recurrent neural networks are usually trained by minimizing an objective  $\mathcal{L}$  that sums all loss contributions incurred over a time horizon of duration  $T$ , namely  $\mathcal{L} = \sum_{t=1}^T \mathcal{L}^t$ , where  $\mathcal{L}^t : \mathbb{R}^o \rightarrow \mathbb{R}$ . The training requires computing the gradient of the objective with respect to parameters  $\mathbf{W}$  [23], namely:

$$\begin{aligned} \frac{\partial \mathcal{L}}{\partial \mathbf{W}} &= \sum_{t=1}^T \frac{\partial \mathcal{L}^t}{\partial \mathbf{W}} \\ \frac{\partial \mathcal{L}^t}{\partial \mathbf{W}} &= \sum_{k=1}^T \text{diag}\left(\frac{\partial \mathcal{L}^t}{\partial \mathbf{y}^k}\right) \frac{\partial \mathbf{y}^k}{\partial \mathbf{W}} \\ \frac{\partial \mathcal{L}^t}{\partial \mathbf{y}^k} &= \left( \frac{\partial \mathcal{L}^t}{\partial \mathcal{E}^t} \frac{\partial \mathcal{E}^t}{\partial \mathbf{y}^t} \frac{\partial \mathbf{y}^t}{\partial \mathbf{y}^k} \right)^T \\ \frac{\partial \mathbf{y}^t}{\partial \mathbf{y}^k} &= \prod_{l=t}^{k+1} \frac{\partial \mathbf{y}^l}{\partial \mathbf{y}^{l-1}} = \prod_{l=t}^{k+1} \text{diag}(g'(\mathbf{z}^l)) \mathbf{W} \end{aligned} \quad (6)$$

where  $\mathbf{z}^l = \mathbf{W} \mathbf{y}^{l-1} + \mathbf{W}_{in} \mathbf{x}^l + \mathbf{b}$  is the vector of logits.

By exploiting the fact that for any real matrices  $\mathbf{A}$ ,  $\mathbf{B}$  and for any real vector  $\mathbf{v}$ ,  $\|\mathbf{A} \mathbf{v}\|_2 \leq \|\mathbf{A}\|_* \|\mathbf{v}\|_2$  and  $\|\mathbf{A} \mathbf{B}\|_* \leq \|\mathbf{A}\|_* \|\mathbf{B}\|_*$ , where  $\|\cdot\|_*$  is the operator-2 norm, it is possible

<sup>8</sup>. This is a common assumption used in the theory of neural networks [57].

to derive an upper-bound on the gradient norm  $\|\frac{\partial \mathcal{L}^t}{\partial \mathbf{y}^k}\|_2$ . In fact,

$$\begin{aligned} \left\| \frac{\partial \mathcal{L}^t}{\partial \mathbf{y}^k} \right\|_2 &= \left\| \frac{\partial \mathcal{L}^t}{\partial \mathcal{E}^t} \frac{\partial \mathcal{E}^t}{\partial \mathbf{y}^t} \frac{\partial \mathbf{y}^t}{\partial \mathbf{y}^k} \right\|_2 \\ &\leq \left\| \frac{\partial \mathcal{L}^t}{\partial \mathcal{E}^t} \right\|_2 \left\| \frac{\partial \mathcal{E}^t}{\partial \mathbf{y}^t} \right\|_* \left\| \frac{\partial \mathbf{y}^t}{\partial \mathbf{y}^k} \right\|_* \\ &\leq \left\| \frac{\partial \mathcal{L}^t}{\partial \mathcal{E}^t} \right\|_2 \left\| \frac{\partial \mathcal{E}^t}{\partial \mathbf{y}^t} \right\|_* \prod_{l=t}^{k+1} \left\| \frac{\partial \mathbf{y}^l}{\partial \mathbf{y}^{l-1}} \right\|_* \end{aligned} \quad (7)$$

Note that from (6) and (7), we can derive the following relations:

$$\begin{aligned} \left\| \frac{\partial \mathbf{y}^l}{\partial \mathbf{y}^{l-1}} \right\|_* &\leq \| \text{diag}(g'(z^l)) \|_* \|\mathbf{W}\|_F \\ &= \max_{i=1, \dots, h} \{g'(z_i^l)\} \|\mathbf{W}\|_F \\ &\leq \frac{\|\mathbf{W}\|_F}{4} \end{aligned} \quad (8)$$

In particular, the first inequality in (8) can be obtained using the property  $\|\mathbf{A}\|_* \leq \|\mathbf{A}\|_F$ , where  $\|\cdot\|_F$  is the Frobenius norm. The equality in second line follows directly from the fact that the operator-2 norm of a diagonal matrix is equal to the maximum of its diagonal entries, whereas the last inequality is due to the fact that the derivative of a sigmoid function cannot be larger than 1/4.

By using the result in (8), the gradient in (7) is bounded by the following inequality:

$$\begin{aligned} \left\| \frac{\partial \mathcal{L}^t}{\partial \mathbf{y}^k} \right\|_2 &\leq \left\| \frac{\partial \mathcal{L}^t}{\partial \mathcal{E}^t} \right\|_2 \left\| \frac{\partial \mathcal{E}^t}{\partial \mathbf{y}^t} \right\|_* \prod_{l=t}^{k+1} \frac{\|\mathbf{W}\|_F}{4} \\ &= \left\| \frac{\partial \mathcal{L}^t}{\partial \mathcal{E}^t} \right\|_2 \left\| \frac{\partial \mathcal{E}^t}{\partial \mathbf{y}^t} \right\|_* \left( \frac{\|\mathbf{W}\|_F}{4} \right)^{t-k-1} \end{aligned} \quad (9)$$

The vanishing gradient problem refers to the decay of  $\|\frac{\partial \mathcal{L}^t}{\partial \mathbf{y}^k}\|_2$  as the number of time instants  $t-k$ , or equivalently the number of layers, becomes larger. A sufficient condition for the occurrence of this problem is given by the condition  $\|\mathbf{W}\|_F < 4$ , due to the fact that the bound in (9) tends to zero as  $t-k \rightarrow \infty$ .

Note that  $\|\mathbf{W}\|_F = \sqrt{\sum_{i=1}^h \|\mathbf{w}_i\|_2^2}$ , where  $\mathbf{w}_i$  is the  $i$ -th row of matrix  $\mathbf{W}$  corresponding to the weights of the  $i$ -th neuron. Furthermore, by the conditions derived in Section 4, viz.  $\|\mathbf{w}_i\|_2^2 = \pi/(2k)$  for all  $i = 1, \dots, h$ , we have that

$$\|\mathbf{W}\|_F = \sqrt{\frac{\pi h}{2k}} \quad (10)$$

If the number of hidden neurons is less than the quantity  $h_{critical} \doteq 32k/\pi$ , which implies that (10) is less than 4, then the vanishing gradient problem is guaranteed to occur. In this case,  $k$  refers to the output variance of a sigmoid activation and is less than or equal to 1/4 (derived from the fact that the output density of a neuron is limited by a Bernoulli distribution and its maximum variance is 1/4, see Section 3). Therefore,  $h_{critical} \leq 8/\pi \approx 2.55$ .

This means that the sufficient condition for the occurrence of the vanishing gradient problem is met only when the number of hidden neurons is less than 3. In practical cases, this limit is overcome with a very large margin,

given that real-world applications usually require hundreds/thousands of hidden neurons per layer. Therefore, even if we cannot conclude that the whole training is exempt of vanishing gradients problems, we initialize the process with a sufficient margin to prevent the problem in the initial phase, which is typically the most critical. Experimental results will provide evidence of this, as shown later in the paper.

## 6 EXPERIMENTAL RESULTS

In this section, we evaluate the performance of the proposed initialization theory on several benchmarks. We start by analyzing shallow networks, then consider the case of deep networks and finally extend the analysis to recurrent neural networks (RNNs, being even deeper than previous cases). We compare our initialization against several competitors. Hereunder, we provide a summary of all strategies:

- Lecun et al. [57] initialize the weights according to  $w_{ij}^l \sim U\left(-\frac{1}{\sqrt{n^l}}, \frac{1}{\sqrt{n^l}}\right)$ , where  $w_{ij}^l$  is the weight connecting neuron  $i$  with neuron  $j$  in layer  $l$  and  $n^l$  is the number of input neurons to layer  $l$ . The biases are set to zero.
- Glorot and Bengio [21] (also known as ‘‘Xavier initialization’’) initialize the weights according to  $w_{ij}^l \sim U\left(-\frac{\sqrt{6}}{\sqrt{n^l+n^{l+1}}}, \frac{\sqrt{6}}{\sqrt{n^l+n^{l+1}}}\right)$ . The biases are set to zero.
- Saxe et al. [51] propose an initialization where each weight matrix is randomly generated from the family of orthogonal matrices, namely  $\mathbf{W}^l$  is satisfying the relation  $\mathbf{W}^{lT} \mathbf{W}^l = \mathbf{I}$ . The biases are set to zero.
- Mishkin and Matas [52] extend the initialization of Saxe et al. by normalizing the weight matrix by the output variance in each layer. The biases are set to zero.
- Our approach exploits the result of Theorem 1 in Section 4, and initializes the weights according to  $w_{ij}^l = \sqrt{\frac{\pi}{2k}} \frac{\tilde{w}_{ij}^l}{\|\tilde{\mathbf{w}}_j^l\|_2}$ ,<sup>9</sup> where  $\tilde{w}_{ij}^l$  can be obtained by using either random generation, namely  $\tilde{w}_{ij}^l \sim U(-1, 1)$ , or the orthogonal initialization in [51]. The biases are set according to  $b_j^l = -\sum_{i=1}^{n^l} w_{ij}^l E\{x_i^l\}$ , where  $E\{x_i^l\}$  is the expected value of input neuron  $x_i^l$ .

In the experiments, we use *lecun*, *glorot*, *ortho* and *lsuv* to identify the results achieved by [57], [21], [51] and [52], respectively. *random+EP* and *ortho+EP* are instead used to identify the two versions of our initialization procedure. In this case, the acronym *EP* stands for *elliptical projection* (see Section 4 for a detailed discussion).

All experiments presented in the next sections are run on a Linux machine equipped by 4 cpu @ 3.2 GHz, 16 GB RAM and a GPU card (NVIDIA TITAN X).

### 6.1 XOR Case: Shallow Network

In this experiment, we generate 200 samples from four 2-dimensional Gaussians. Classes are assigned to create a XOR

9.  $k \doteq \text{Var}\{x\} \approx 0.0589$ , where  $\text{Var}\{x\}$  is computed numerically using  $p_y(y)$  at optimality ( $x$  is therefore the output of the previous neuron).

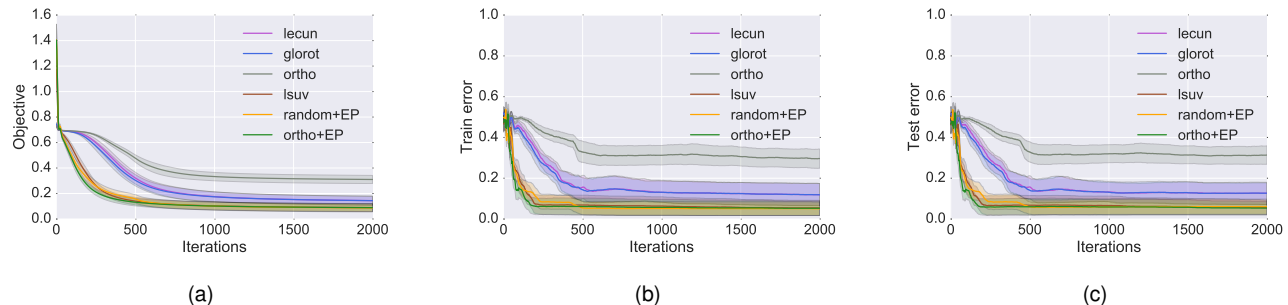


Fig. 4. Learning curves for (a) training objective, (b) training error and (c) test error on the XOR case over different initialization methods.

TABLE 1

Quantitative results on MNIST with shallow network [59] and different initialization strategies

Method (*sigmoid)	T.E. (%)	Train Time ( $10^3$ secs)
lecun*	$1.91 \pm 0.03$	2.0
glorot*	$1.86 \pm 0.04$	2.0
ortho*	$1.86 \pm 0.02$	2.0
lsuv*	$1.87 \pm 0.01$	2.0
ortho+EP*	$1.89 \pm 0.02$	2.0
random+EP*	<b><math>1.78 \pm 0.06</math></b>	2.0

TABLE 2

Quantitative results on MNIST with shallow network [59] and dropout ( $p = 0.5$ ) for different initialization strategies

Method (*sigmoid)	T.E. (%)	Train Time ( $10^3$ secs)
[59]	<b>1.60</b>	-
lecun*	$1.65 \pm 0.03$	6.0
glorot*	$1.63 \pm 0.02$	6.0
ortho*	<b><math>1.62 \pm 0.04</math></b>	6.0
lsuv*	<b><math>1.61 \pm 0.03</math></b>	6.0
ortho+EP*	<b><math>1.61 \pm 0.03</math></b>	6.0
random+EP*	<b><math>1.59 \pm 0.03</math></b>	6.0

configuration. In this case, we use a neural network with one hidden layer containing two hidden units. This is the smallest network that can learn correctly the problem (4 modes can be represented more compactly with 2 binary digits, namely 2 hidden neurons). Gradient descent with momentum equal to 0.9 and learning rate equal to 0.05 is applied to the minimization of the cross-entropy objective function. Fig. 4 shows results over ten repeated experiments (generating new data from the same distribution and initializing the network differently). It is clear from these experiments that our proposed initialization allows to achieve the best solution in a very efficient way. Also, *lsuv* is able to achieve comparable performance to our method. Moreover, it’s interesting to note that *ortho* obtains the worst performance, in fact the test error rate, viz. T.E., is about 25%, meaning that this initialization is not particularly suited for this non-linear separable scenario.

## 6.2 MNIST: Shallow Network

In this section, we compare different initialization methods for a shallow network with 800 hidden units characterized by sigmoid activation functions and with softmax output

layer on the MNIST benchmark dataset [60]. Mini-batch gradient descent with momentum equal to 0.9 and learning rate equal to 0.001 is applied to the minimization of the cross-entropy objective function. The size of each mini-batch consists of 50 training samples and the training algorithm is run for 900k iterations. All results, including the learning curves, are averaged over 4 different random initializations. Data is normalized and mean-centered to lie in the range  $[-1, 1]$ .

We plot the training curves for the objective computed on both the training and the validation sets, see Fig. 5. We see that our proposed initialization scheme allows to converge faster even in the case of non-deep models. Furthermore, our strategy is quite robust to the initial generation of weights. Previous attempts have shown that random initializations produces solutions with very different performance, thus requiring very expensive pre-processing strategies to reduce the variance of generalization estimates, like unsupervised pre-training [33]. To the best of our knowledge, this is the very first time that random initialization without unsupervised pre-training allows to converge to solutions with reduced variance in performance (see *random+EP* Fig. 5a and Fig. 5d).

In Table 1, we show the test errors with the related training times.<sup>10</sup> Model selection is performed based on the minimization of the validation objective. The performance in terms of generalization are pretty similar for all methods, thus the main advantage of our strategy consists of faster convergence.

We apply also dropout [61] (where the dropping probability is set to 0.5) and compare with the state of the art results reported in [59], which are obtained with the same network architecture, but with hand-crafted activation functions. In particular, the authors use squashed hyperbolic tangent activations, defined as  $f(z) = \text{Atanh}(Bz)$ , where  $A = 1.7159$  and  $B = 2/3$  (the parametrization derives by the requirement that  $f(1) = 1$  and  $f(-1) = -1$ ), because their function gain is close to 1 in the nominal region and the computed gradients are therefore less attenuated [60] compared to sigmoids. Table 2 summarizes the results. To the best of our knowledge, this is the first experimental trial demonstrating that sigmoids achieve similar performance to hyperbolic tangents [59].

<sup>10</sup> All training times are equal, since they represent the time to perform all training epochs.

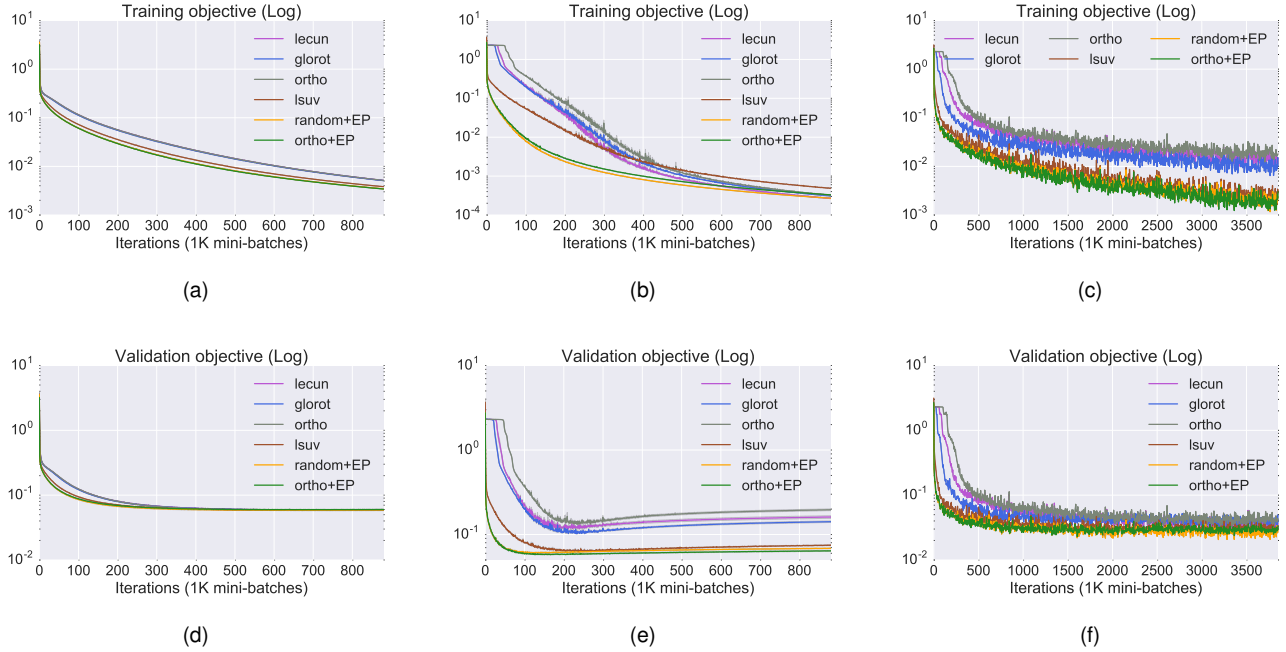


Fig. 5. Learning curves for training and validation objectives on MNIST (logarithmic scale): (a) and (d) results with shallow network, (b) and (e) results with deep network, (c) and (f) results with deep network with data augmentation.

TABLE 3

Quantitative results on MNIST with deep network [62] and different initialization strategies

Method (*sigmoid)	T.E. (%)	Train Time ( $10^3$ secs)
lecun*	$3.11 \pm 0.14$	7.3
glorot*	$2.94 \pm 0.08$	7.3
ortho*	$3.32 \pm 0.11$	7.3
lsuv*	$2.07 \pm 0.07$	7.3
ortho+EP*	<b><math>1.85 \pm 0.07</math></b>	7.3
random+EP*	<b><math>1.92 \pm 0.08</math></b>	7.3

TABLE 4

Quantitative results on MNIST with deep network [62] and data augmentation for different initialization strategies

Method (*sigmoid)	T.E. (%)	Train Time ( $10^3$ secs)
[62]	0.32	412.2
[62] <sup>+</sup>	<b>0.62</b>	35.4
lecun*	0.80	35.4
glorot*	0.82	35.4
ortho*	0.80	35.4
lsuv*	0.79	35.4
ortho+EP*	0.81	35.4
random+EP*	<b>0.68</b>	35.4

<sup>+</sup> Our implementation

### 6.3 MNIST: Deep Network

We repeat the experiments of previous subsection with same setup, but with a deeper network. In particular, we use the same architecture of [62], consisting of 6 layers (5 hidden and 1 output layer), where the number of neurons in each layer is chosen according to a pyramidal structure, namely 2500, 2000, 1500, 1000, 500 and 10 neurons, respectively.

From Fig. 5b and Fig. 5e, we observe immediately that our initialization provides a gain in terms of both convergence speed and the quality of the obtained solution. It is also interesting to see that the competitors observe very slow learning in the early stages of training, probably due to the fact that the network parameters are initialized on flat regions of the training objective and the gradients are therefore vanishing.

We also analyze the evolution of the statistics of each layer over the first 90k iterations (we consider the mean and the standard deviation of each layer obtained by averaging neuron activities over mini-batches). Fig. 6 shows the behaviour of the network for different initialization strategies. For almost all competitors, the activities in the last hidden layer (layer 5) tend to be biased towards zero and no sig-

nificant variation is appreciated in the output layer. This is a symptomatic behaviour, that have been already observed in [21] for networks with standard logistic activations. It is interesting to mention that this problem is not visible for *lsuv* and our proposed initializations. This is probably due to the fact that both impose some conditions on the variance of the weights of each neuron. In particular, *lsuv* imposes a unit variance, while our conditions require a larger value, which is based on an information-theoretically criterion. This has also some beneficial impact on the generalization performance as shown in Table 3. Therefore, our weight initialization is sufficient to guarantee a better propagation of gradients at all layers for the whole training process, allowing to achieve faster convergence and better solutions.

We apply also data augmentation to compare against the state of the art results reported in [62] with squashed hyperbolic tangent activations. In particular, training data are augmented following the methodology suggested in [62]. We use elastic distortion, to emulate uncontrolled oscillations of

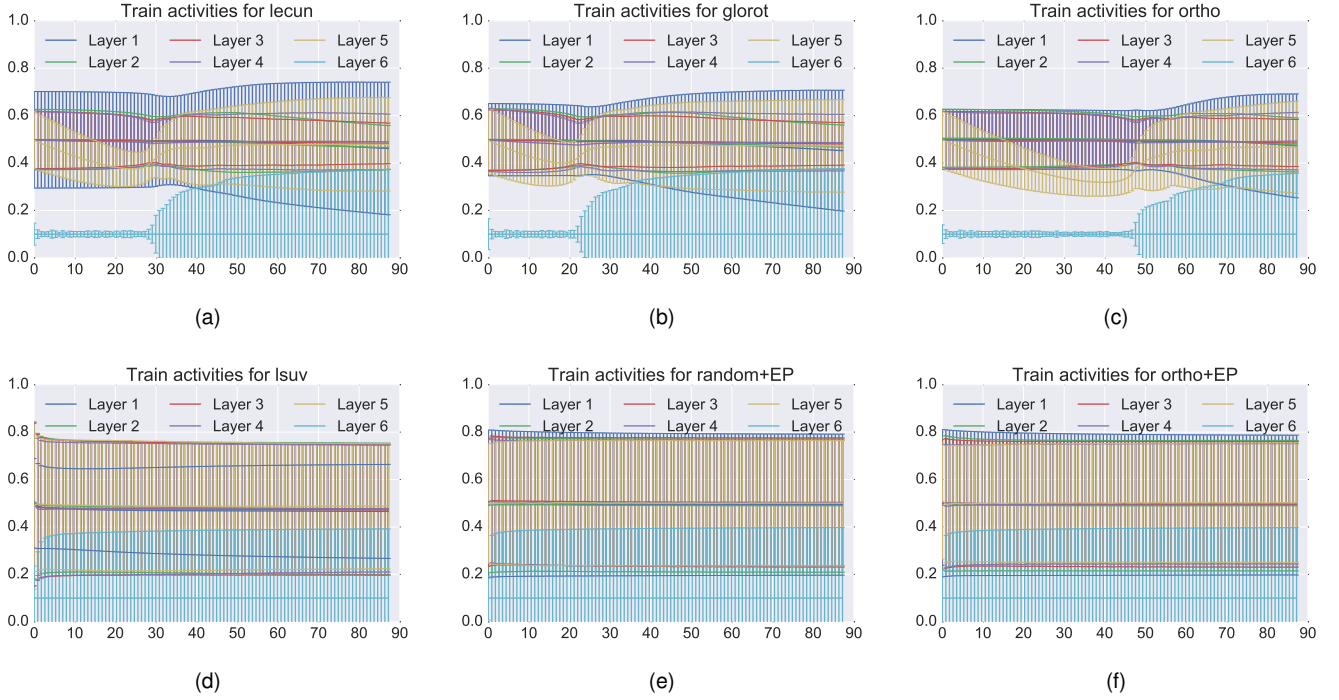


Fig. 6. Temporal evolution of statistics (mean and standard deviation) of activations in each layer for different initialization methods over the first 90k iterations.

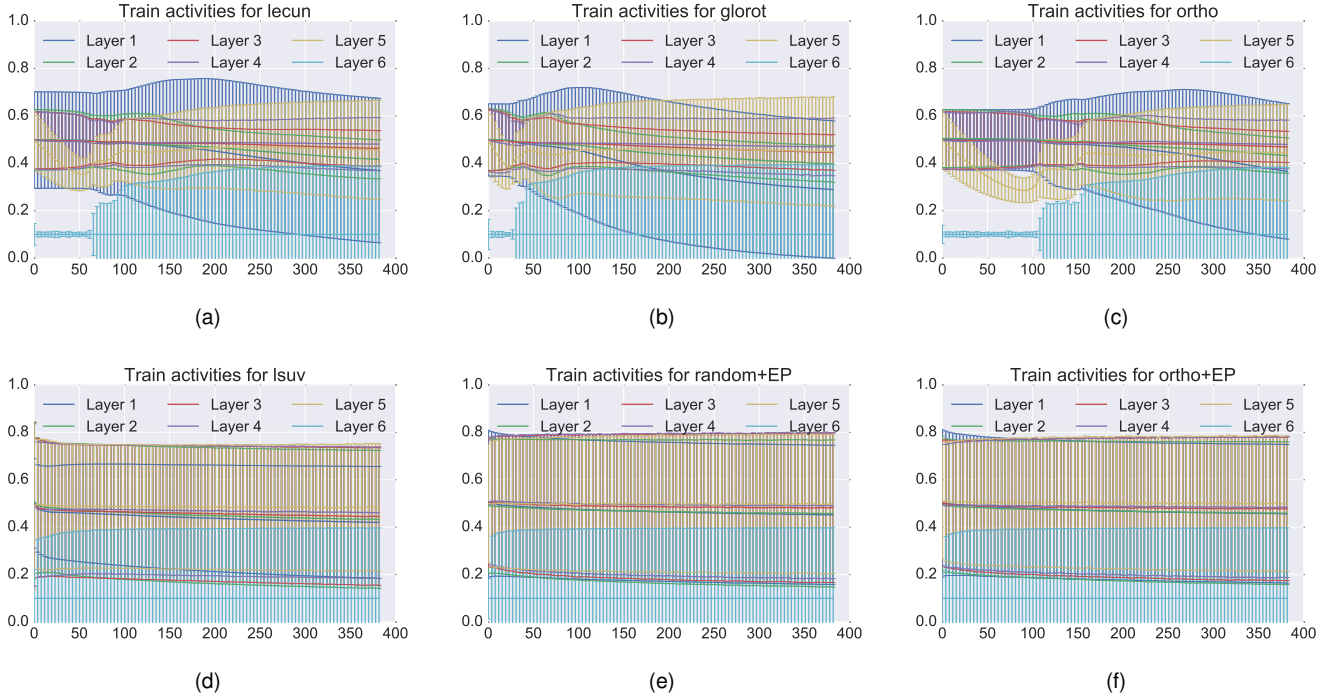


Fig. 7. Temporal evolution of statistics (mean and standard deviation) of activations in each layer for different initialization methods over the first 90k iterations. Data augmentation is applied to improve performance.

hand muscles ( $\sigma = 5.5$  and  $\alpha = 37$ , see [62]),<sup>11</sup> rotation (with an angle randomly sampled from  $[-\beta, \beta]$ , where  $\beta = 7.5$  for digits 1 and 7 and  $\beta = 15$  for all other digits) and horizontal and vertical scaling (with scaling factor randomly sampled

from  $[1 - \gamma/100, 1 + \gamma/100]$ , where  $\gamma = 17.5$ ). We also rerun the experiments of [62] and use these as baseline, since we were not able to replicate the results.

The learning curves in Fig. 5c and Fig. 5f confirms the findings that our method achieves faster convergence and better solutions. It is important to mention that the use of

11. Here,  $\sigma$  does not refer to  $\sigma$  introduced in Section 3.

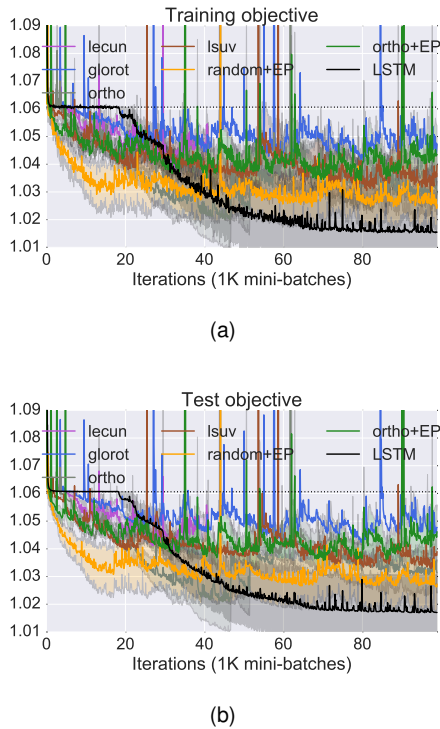


Fig. 8. Training and test learning curves on the copy memory problem for different strategies.

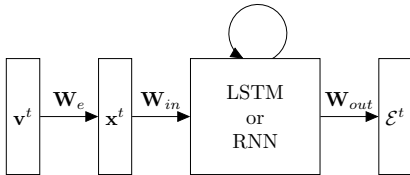


Fig. 9. General architecture used in the experiments with recurrent neural networks.  $\mathbf{v}^t$ ,  $\mathcal{E}^t$  are the input and the output vectors, respectively, representing a character or a word using one-hot encoding, while  $\mathbf{x}^t$  represents the distributed embedding of the input vector.

data augmentation plays an important role in achieving better generalization performance and that it can partially overcome to problems incurred by using a wrong initialization. Nevertheless, the advantages of our initialization are still visible. Fig. 7 shows the temporal evolution of statistics for each layer, emphasizing the fact that almost all competitors are subject to the problem of saturation of the last hidden layer in the early stages of training [21]. Table 4 summarizes the quantitative results. Our initialization strategy (*random+EP*) allows to achieve 0.68% of test error rate, which is very close to the performance (namely 0.62%) obtained by using the hand-crafted hyperbolic tangent of [62]. This provides further evidence that deep networks with standard logistic activations can perform similarly to networks with hyperbolic tangents and that the training is made feasible through some simple conditions at initialization.

## 6.4 Copying Memory Problem: Recurrent Neural Network

In this section, we go even deeper and use RNNs as case study to compare the different initialization strategies. It is well known that these models have difficulties to remember information about inputs for long time intervals. This is due to the fact that during training, RNNs are affected by the problem of vanishing/exploding gradients [29], [58]. The literature contains a plethora of proposed solutions. In particular, the authors in [63], [64] propose a strategy called Echo-State Networks (ESN), which consist in carefully initializing the recurrent weights and training only the output parameters. In practice, the recurrent weight matrix is initialized to have a spectral radius close to one, such that inputs can “echo” for long time. This represents a very drastic solution, which doesn’t exploit the full potential of RNNs. Authors in [65] show that long-term dependencies can be learnt using Hessian-free optimization, which is provided with information about the curvature of the loss surface and is therefore able to deal with vanishing gradients. Authors in [58] propose a solution to train RNNs, where a regularizer, specifically designed to cope with vanishing gradients, is applied to the loss objective and a simple momentum-based optimizer is used in combination with gradient clipping, that ensures that gradients do not explode. In our experiments, we use the same strategies of [58] and we focus on analyzing the impact of initialization on this problem. It is also important to mention that there is a recent line of research in RNNs, studying unitary recurrent weight matrices, see for example [66], [67], [68]. Nevertheless, in this work we want to study the most general case, where the feasible set consists of the whole parameter space.

In order to study the capability of models in learning long-term dependencies, we consider a similar pathological task introduced for the first time in [69], called the copy memory problem. In this task, we are given a dictionary of ten characters, viz.  $\{a_i\}_{i=0}^9$ . The input is a  $T + 6$  length sequence containing characters from the dictionary. Specifically, the first three characters in the sequence are drawn uniformly and independently with replacement from the subset  $\{a_i\}_{i=0}^7$  and represent the sequence to be memorized. The next  $T - 1$  characters are set to  $a_8$  and represent a dummy sequence. The next character is set to  $a_9$  and represent a trigger to inform the model that it should start to predict the memorized sequence. The last three characters are set to  $a_8$  and represent a dummy sequence. The ground truth output is a  $T + 6$  length sequence, where the first  $T + 3$  entries are set to  $a_8$  and the last three characters are the copy of the first characters in the input sequence. Therefore, the task consists in memorizing the input sequence for  $T$  time instants and then output the memorized sequence. In the experiments, we set  $T = 100$  and generate training and test datasets consisting of 1000 samples each.

We compare RNNs using different initialization strategies and report also the results of two baselines. The first baseline consists in outputting  $a_8$  for the first  $T + 3$  entries and randomly sampling from the subset  $\{a_i\}_{i=0}^7$  for the last three characters. This is equivalent to having a *memoryless* strategy. The second baseline consists in predicting the output using a LSTM model [69], which is the most widely used

TABLE 5  
Quantitative results on the language modelling task for different strategies.

Method (*sigmoid)	T.P.	Train Time ( $10^3$ secs)
lstm	<b>128.3±0.5</b>	77.0
lecun*	143.1±0.8	28.7
glorot*	155.1±0.9	28.7
ortho*	156.1±0.5	28.7
lsuv*	<b>135.9±0.1</b>	28.7
ortho+EP*	<b>135.5±0.3</b>	28.7
random+EP*	164.0±0.5	28.7

alternative to RNNs and is able to learn long-term dependencies. Performance are measured in terms of perplexity and this quantity is also used as training objective. Note that the perplexity of the first baseline can be analytically computed and is equal to  $\exp\left\{\frac{3 \ln 8}{T+6}\right\} \approx 1.06$ .

The network architecture used in the experiments is shown in Fig. 9, where the input and the output vectors represent the one-hot encoding of any character in the dictionary. The size of hidden layers in the recurrent model (which is also used to determine the size of the embedding vector) depends whether we are using RNN or LSTM. In particular, RNN and LSTM have hidden layers of size 100 and 52, respectively, which is equivalent to have roughly 32000 parameters per model. Adam optimizer with learning rate equal to 0.001 is used in training and the algorithm is run for 100k iterations. All results are averaged over 4 different random initializations.

Figure 8 shows the learning curves for the different initialization strategies as well as the learning curves of the two baselines. It is possible to see that eventually all approaches perform better than the *memoryless* strategy, meaning that the networks effectively learn to memorize some information. Furthermore, our initialization (*random+EP*) outperforms all other approaches during the first 30k iterations, including LSTM. There is a phase between 30k and 50k iterations, in which *ortho* achieves the best performance. As discussed in [51], an orthogonal initialization can guarantee that the recurrent weight matrix remains orthogonal during the whole training process even in the case of nonlinear activation functions. This is particularly useful in the copying memory problem, since the family of orthogonal matrices contain the solution, that allows the RNN to learn the identity function, namely to copy the exact input sequence to the output. Note that after 50k iterations the performance of *ortho* degrades due to the problem of exploding gradients. It is interesting to note that at convergence we achieve the best performance among the other initializations and are able to get closer to the results of LSTM.

## 6.5 Language modelling: Recurrent Neural Network

In this section, we conduct experiments on a real-world task, namely the language modelling problem, using the Penn Tree Bank (PTB) dataset [70]. The dataset consists of 929k training words, 73k validation words, 82k test words and the vocabulary has 10k words. The dataset is downloaded from Tomas Mikolov’s webpage.<sup>12</sup>

12. <http://www.fit.vutbr.cz/~imikolov/rnnlm/simple-examples.tgz>

TABLE 6  
Quantitative results on the language modelling task for different strategies with dropout.

Method (*sigmoid)	T.P.	Train Time ( $10^3$ secs)
lstm	<b>128.7±0.4</b>	80.0
lecun*	147.8±0.6	32.3
glorot*	159.2±0.4	32.3
ortho*	161.2±0.3	32.3
lsuv*	139.8±0.4	32.3
ortho+EP*	139.3±0.3	32.3
random+EP*	<b>130.1±0.4</b>	32.3

We compare RNNs using different initialization strategies and report also the results of the baseline using LSTM [69]. The aim of these experiments is to show that our conditions allow to improve the generalization performance of RNNs. With our initialization, we are able to achieve comparable performance to the one obtained by LSTM.

The network architecture is the same as the one used in the copying memory problem with different size of the hidden layers. In particular, we use 200 neurons for RNNs and 190 neurons for LSTM. This corresponds to have roughly 4090k parameters for each model.

Adam optimizer with learning rate equal to 0.0001 and gradient clipping [58] is used for training the models and the algorithm is run for 500k iterations.

Results are averaged over 4 different random initializations and are shown in Table 5 (the acronym T.P. stands for test perplexity). *lsuv* and *ortho+EP* achieve performance closer to the ones of LSTM, while *random+EP* obtains apparently very bad performance. We argue that the generation of the initial matrices in *random+EP* allows to sample from a much larger space of matrices and consequently Adam has more chances to overfit. Note that the problem of overfitting of the Adam optimizer is known and is discussed from a theoretical perspective in [47]. To validate this claim and potentially reduce the problem of overfitting, we run also the experiments with dropout following the procedure in [71], where the dropping probability is set to 0.5. Results, shown in Table 6, confirm our initial claim. *random+EP* outperforms all other initialization and is able to achieve performance comparable to LSTM. Note that RNNs offer a clear advantage in terms of computational complexity over LSTM, as demonstrated by the training times in Table 6.

## 7 CONCLUSION

This work shows that a careful initialization of the parameters is sufficient to successfully train feedforward neural networks with standard logistic activations. The initialization is based on some conditions, that are derived by studying the properties of a single neuron through information theory. The study is corroborated by numerous experiments over different known benchmarks and different networks.

## APPENDIX A DERIVATION OF BOUNDS (3)

Recall that

$$H(y) = H(z) + E_z\{\ln g'(z)\} \quad (11)$$

where (we drop the extrema of integration for the sake of brevity in the notation)

$$\begin{aligned} H(z) &\doteq - \int \mathcal{N}(\mu, \sigma^2) \ln \mathcal{N}(\mu, \sigma^2) dz \\ &= \frac{1}{2\sigma^2} \int (z - \mu)^2 \mathcal{N}(\mu, \sigma^2) dz + \ln(\sqrt{2\pi\sigma^2}) \\ &= \frac{1}{2} + \frac{1}{2} \ln(2\pi\sigma^2) \end{aligned} \quad (12)$$

and

$$\begin{aligned} E_z \{\ln g'(z)\} &\doteq \int \mathcal{N}(\mu, \sigma^2) \ln g'(z) dz \\ &= \int \mathcal{N}(\mu, \sigma^2) \ln [g(z)(1 - g(z))] dz \\ &= \int \mathcal{N}(\mu, \sigma^2) \ln \left[ \frac{e^z}{(1 + e^z)^2} \right] dz \\ &= \int z \mathcal{N}(\mu, \sigma^2) dz - 2 \int \mathcal{N}(\mu, \sigma^2) \ln(1 + e^z) dz \\ &= \mu - 2 \int \mathcal{N}(\mu, \sigma^2) \ln(1 + e^z) dz \end{aligned} \quad (13)$$

Note that the integrand in (13) is always positive and that  $\max(0, z) < \ln(1 + e^z) \leq \max(0, z) + \ln 2$  is true for any  $z$ . Therefore, we can easily derive the following relations, namely:

$$A(\mu, \sigma) - 2 \ln 2 \leq E_z \{\ln g'(z)\} < A(\mu, \sigma) \quad (14)$$

where

$$\begin{aligned} A(\mu, \sigma) &\doteq \mu - 2 \int_{-\infty}^{\infty} \mathcal{N}(\mu, \sigma^2) \max(0, z) dz \\ &= \mu - 2 \int_0^{\infty} z \mathcal{N}(\mu, \sigma^2) dz \\ &= \mu - \mu - \mu \operatorname{erf}\left(\frac{\mu}{\sigma\sqrt{2}}\right) - \frac{2\sigma}{\sqrt{2\pi}} e^{-\frac{\mu^2}{2\sigma^2}} \\ &= -\mu \operatorname{erf}\left(\frac{\mu}{\sigma\sqrt{2}}\right) - \frac{2\sigma}{\sqrt{2\pi}} e^{-\frac{\mu^2}{2\sigma^2}} \end{aligned} \quad (15)$$

By adding  $H(z)$  to (14) and using (11), we obtain that

$$\begin{aligned} H(z) + A(\mu, \sigma) - 2 \ln 2 &\leq H(y) < H(z) + A(\mu, \sigma) \\ H_B(\mu, \sigma) - 2 \ln 2 &\leq H(y) < H_B(\mu, \sigma) \end{aligned} \quad (16)$$

where  $H_B(\mu, \sigma) \doteq H(z) + A(\mu, \sigma)$ .

## APPENDIX B PROOF OF THEOREM 1

Recall the definition of the lower bound in (4), namely:

$$H_B(\mu, \sigma) \doteq \frac{1}{2} + \ln(\sqrt{2\pi\sigma^2}) - \mu \operatorname{erf}\left(\frac{\mu}{\sigma\sqrt{2}}\right) - \frac{2\sigma}{\sqrt{2\pi}} e^{-\frac{\mu^2}{2\sigma^2}}$$

By the fact that  $\frac{d \operatorname{erf}(t)}{dt} = \frac{2}{\sqrt{\pi}} e^{-t^2}$  and using standard calculus of derivatives, we can get that:

$$\begin{aligned} \frac{\partial H_B(\mu, \sigma)}{\partial \mu} &= -\operatorname{erf}\left(\frac{\mu}{\sigma\sqrt{2}}\right) \\ \frac{\partial H_B(\mu, \sigma)}{\partial \sigma} &= \frac{1}{\sigma} - \frac{2}{\sqrt{2\pi}} e^{-\frac{\mu^2}{2\sigma^2}} \end{aligned}$$

where the first line is zero if and only if  $\mu = 0$ , thus proving the first condition in Theorem 1, while, by setting the second line to zero, we obtain the following equation:

$$\frac{e^{-\frac{\mu^2}{2\sigma^2}}}{\sigma} = \frac{2}{\sqrt{2\pi}} \quad (17)$$

By the change of variable  $t \doteq \frac{\mu}{\sigma\sqrt{2}}$ , (17) simplifies in the following equation:

$$te^{t^2} = \frac{\mu}{\sqrt{\pi}} \quad (18)$$

whose solution is given by:

$$t = \frac{\mu}{\sqrt{\pi}} e^{-W\left(\frac{2\mu^2}{\pi}\right)} \quad (19)$$

where  $W(\cdot)$  is the principal branch of the Lambert W function [56]. We can check whether (19) is the solution of (18), by substituting (19) in (18) and see that the equality (18) holds, namely:

$$\begin{aligned} \frac{\mu}{\sqrt{\pi}} e^{-\frac{W\left(\frac{2\mu^2}{\pi}\right)}{2}} e^{\frac{\mu^2}{\pi} e^{-W\left(\frac{2\mu^2}{\pi}\right)}} &= \frac{\mu}{\sqrt{\pi}} \\ e^{-\frac{W\left(\frac{2\mu^2}{\pi}\right)}{2}} e^{\frac{\mu^2}{\pi} e^{-W\left(\frac{2\mu^2}{\pi}\right)}} &= 1 \\ e^{-\frac{W\left(\frac{2\mu^2}{\pi}\right)}{2}} e^{\frac{2\mu^2}{\pi} e^{-W\left(\frac{2\mu^2}{\pi}\right)}} &= 1 \\ e^{-\frac{W\left(\frac{2\mu^2}{\pi}\right)}{2}} e^{\frac{W\left(\frac{2\mu^2}{\pi}\right)}{2}} &= 1 \end{aligned}$$

where the fourth line is obtained by the identity  $t = W(t)e^{W(t)}$ , or equivalently  $te^{-W(t)} = W(t)$ . Therefore, solution (19) can be explicitated in terms of  $\sigma$ , thus giving us the second condition in Theorem 1.

To prove the optimality of the the obtained solution, we perform a second-order derivative test, namely:

$$\begin{aligned} \frac{\partial^2 H_B(\mu, \sigma)}{\partial \mu^2} &= -\sqrt{\frac{2}{\pi}} \frac{1}{\sigma} e^{-\frac{\mu^2}{2\sigma^2}} \\ \frac{\partial^2 H_B(\mu, \sigma)}{\partial \sigma^2} &= -\frac{1}{\sigma^2} - \sqrt{\frac{2}{\pi}} \frac{\mu^2}{\sigma^2} e^{-\frac{\mu^2}{2\sigma^2}} \\ \frac{\partial^2 H_B(\mu, \sigma)}{\partial \mu \partial \sigma} &= \frac{\partial^2 H_B(\mu, \sigma)}{\partial \sigma \partial \mu} = \sqrt{\frac{2}{\pi}} \frac{\mu}{\sigma^2} e^{-\frac{\mu^2}{2\sigma^2}} \end{aligned} \quad (20)$$

Note that the first two equations in (20) are always negative, while the third equation is zero at  $\mu = 0$ . Therefore the Hessian matrix for the obtained stationary point is negative-definite. Q.E.D.

## APPENDIX C GENERAL CASE OF DIFFERENT INPUT VARIANCES

Suppose that we are given an initial weight vector denoted by  $\tilde{\mathbf{w}} \in \mathbb{R}^d$ . In general,  $\tilde{\mathbf{w}}$  does not satisfy the optimality condition given by Theorem 1, namely  $\sum_{i=1}^d \tilde{w}_i^2 \operatorname{Var}\{x_i\} \neq \pi/2$ . We need to find the closest vector to  $\tilde{\mathbf{w}}$  that satisfies the condition in order to have maximum amount of information propagation. This can be formulated as the following optimization problem:

$$\begin{aligned} \min_{\mathbf{w}} & \|\mathbf{w} - \tilde{\mathbf{w}}\|_2^2 \\ \text{s.t.} & \mathbf{w}^T \mathbf{D} \mathbf{w} = \pi/2 \end{aligned} \quad (21)$$

where  $\mathbf{D} \doteq \text{diag}(\text{Var}\{x_1\}, \dots, \text{Var}\{x_d\})$  and the solution can be obtained by using existing iterative non-convex optimization procedures, due to the fact that the feasible set in (21) is not convex.

## ACKNOWLEDGMENTS

We gratefully acknowledge NVIDIA Corporation with the donation of a Titan X Pascal machine to support this research. We thank Massimo Zanetti for insightful discussion.

## REFERENCES

- [1] R. Girshick, J. Donahue, T. Darrell, and J. Malik, "Region-Based Convolutional Networks for Accurate Object Detection and Segmentation," *TPAMI*, vol. 38, no. 1, pp. 142–158, 2016.
- [2] S. Ji, W. Xu, M. Yang, and K. Yu, "3D Convolutional Neural Networks for Human Action Recognition," *TPAMI*, vol. 35, no. 1, pp. 221–231, 2013.
- [3] C. Dong, C. C. Loy, K. He, and X. Tang, "Image Super-Resolution Using Deep Convolutional Networks," *TPAMI*, vol. 38, no. 2, pp. 295–307, 2016.
- [4] A. Krizhevsky, I. Sutskever, and G. E. Hinton, "Imagenet Classification with Deep Convolutional Neural Networks," in *NIPS*, 2012, pp. 1097–1105.
- [5] R. Jozefowicz, O. Vinyals, M. Schuster, N. Shazeer, and Y. Wu, "Exploring the Limits of Language Modeling," *arXiv preprint arXiv:1602.02410*, 2016.
- [6] O. Vinyals, L. Kaiser, T. Koo, S. Petrov, I. Sutskever, and G. Hinton, "Grammar as a Foreign Language," in *NIPS*, 2015, pp. 2773–2781.
- [7] I. Sutskever, O. Vinyals, and Q. V. Le, "Sequence to Sequence Learning with Neural Networks," in *NIPS*, 2014, pp. 3104–3112.
- [8] A. Graves and N. Jaitly, "Towards End-to-End Speech Recognition with Recurrent Neural Networks," in *ICML*, 2014, pp. 1764–1772.
- [9] N. Kruger, P. Janssen, S. Kalkan, M. Lappe, A. Leonardis, J. Piater, A. J. Rodriguez-Sanchez, and L. Wiskott, "Deep Hierarchies in the Primate Visual Cortex: What Can We Learn for Computer Vision?" *TPAMI*, vol. 35, no. 8, pp. 1847–1871, 2013.
- [10] G. F. Montufar, R. Pascanu, K. Cho, and Y. Bengio, "On the number of linear regions of deep neural networks," in *NIPS*, 2014, pp. 2924–2932.
- [11] M. Raghu, B. Poole, J. Kleinberg, S. Ganguli, and J. Sohl-Dickstein, "On the Expressive Power of Deep Neural Networks," *ICML*, 2017.
- [12] B. Poole, S. Lahiri, M. Raghu, J. Sohl-Dickstein, and S. Ganguli, "Exponential Expressivity in Deep Neural Networks Through Transient Chaos," in *NIPS*, 2016, pp. 3360–3368.
- [13] Y. Bengio *et al.*, "Learning Deep Architectures for AI," *Foundations and trends® in Machine Learning*, vol. 2, no. 1, pp. 1–127, 2009.
- [14] F. Doshi-Velez and B. Kim, "Towards a Rigorous Science of Interpretable Machine Learning," *arXiv preprint arXiv:1702.08608*, 2017.
- [15] B. Goodman and S. Flaxman, "European Union Regulations on Algorithmic Decision-Making and a 'Right to Explanation'," *arXiv preprint arXiv:1606.08813*, 2016.
- [16] P. Dayan and L. F. Abbott, *Theoretical Neuroscience*. Cambridge, MA: MIT Press, 2001, vol. 806.
- [17] D. Hassabis, D. Kumaran, C. Summerfield, and M. Botvinick, "Neuroscience-Inspired Artificial Intelligence," *Neuron*, vol. 95, no. 2, pp. 245–258, 2017.
- [18] J. M. Benítez, J. L. Castro, and I. Requena, "Are Artificial Neural Networks Black Boxes?" *IEEE Transactions on Neural Networks*, vol. 8, no. 5, pp. 1156–1164, 1997.
- [19] S. Mitra and Y. Hayashi, "Neuro-fuzzy Rule Generation: Survey in Soft Computing Framework," *IEEE Transactions on Neural Networks*, vol. 11, no. 3, pp. 748–768, 2000.
- [20] Y. LeCun, L. Bottou, G. B. Orr, and K.-R. Müller, "Efficient Back-Prop," in *NIPS Workshop*. Springer-Verlag, 1998, pp. 9–50.
- [21] X. Glorot and Y. Bengio, "Understanding the Difficulty of Training Deep Feedforward Neural Networks," in *AISTATS*, 2010.
- [22] B. Xu, R. Huang, and M. Li, "Revise Saturated Activation Functions," *ICLR Workshop*, 2016.
- [23] D. E. Rumelhart and G. E. Hinton, "Learning Representations by Back-Propagating Errors," *Nature*, vol. 323, p. 9, 1986.
- [24] J. Schmidhuber, "Deep Learning in Neural Networks: An Overview," *Neural Networks*, vol. 61, pp. 85–117, 2015.
- [25] M. Fernández-Redondo and C. Hernandez-Espinosa, "A Comparison among Weight Initialization Methods for Multilayer Feedforward Networks," in *IJCNN*, vol. 4. IEEE, 2000, pp. 543–548.
- [26] X. M. Zhang, Y. Q. Chen, N. Ansari, and Y. Q. Shi, "Mini-Max Initialization for Function Approximation," *Neurocomputing*, vol. 57, pp. 389–409, 2004.
- [27] G. Cybenko, "Approximation by Superpositions of a Sigmoidal Function," *Mathematics of Control, Signals, and Systems (MCSS)*, vol. 2, no. 4, pp. 303–314, 1989.
- [28] K. Hornik, M. Stinchcombe, and H. White, "Multilayer Feedforward Networks are Universal Approximators," *Neural networks*, vol. 2, no. 5, pp. 359–366, 1989.
- [29] Y. Bengio, P. Simard, and P. Frasconi, "Learning Long-Term Dependencies with Gradient Descent is Difficult," *IEEE Transactions on Neural Networks*, vol. 5, no. 2, pp. 157–166, 1994.
- [30] G. E. Hinton and R. R. Salakhutdinov, "Reducing the Dimensionality of Data with Neural Networks," *Science*, vol. 313, no. 5786, pp. 504–507, 2006.
- [31] Y. Bengio, P. Lamblin, D. Popovici, and H. Larochelle, "Greedy Layer-Wise Training of Deep Networks," in *NIPS*, 2007, pp. 153–160.
- [32] C. Poultney, S. Chopra, Y. L. Cun *et al.*, "Efficient Learning of Sparse Representations with an Energy-Based Model," in *NIPS*, 2007, pp. 1137–1144.
- [33] D. Erhan, Y. Bengio, A. Courville, P.-A. Manzagol, P. Vincent, and S. Bengio, "Why Does Unsupervised Pre-training Help Deep Learning?" *JMLR*, vol. 11, no. Feb, pp. 625–660, 2010.
- [34] K. He, X. Zhang, S. Ren, and J. Sun, "Deep Residual Learning for Image Recognition," in *CVPR*, 2016, pp. 770–778.
- [35] R. K. Srivastava, K. Greff, and J. Schmidhuber, "Highway Networks," *ICML Workshop*, 2015.
- [36] G. Huang, Z. Liu, K. Q. Weinberger, and L. van der Maaten, "Densely Connected Convolutional Networks," *CVPR*, 2017.
- [37] S. Ioffe and C. Szegedy, "Batch Normalization: Accelerating Deep Network Training by Reducing Internal Covariate Shift," in *ICML*, 2015, pp. 448–456.
- [38] J. L. Ba, J. R. Kiros, and G. E. Hinton, "Layer Normalization," *NIPS Deep Learning Symposium*, 2016.
- [39] T. Salimans and D. P. Kingma, "Weight Normalization: A Simple Reparameterization to Accelerate Training of Deep Neural Networks," in *NIPS*, 2016, pp. 901–901.
- [40] B. T. Polyak, "Some Methods of Speeding up the Convergence of Iteration Methods," *USSR Computational Mathematics and Mathematical Physics*, vol. 4, no. 5, pp. 1–17, 1964.
- [41] I. Sutskever, J. Martens, G. Dahl, and G. Hinton, "On the Importance of Initialization and Momentum in Deep Learning," in *ICML*, 2013, pp. 1139–1147.
- [42] D. Kingma and J. Ba, "Adam: A Method for Stochastic Optimization," *ICLR*, 2014.
- [43] J. Martens, "Deep Learning via Hessian-Free Optimization," in *ICML*, 2010, pp. 735–742.
- [44] S.-I. Amari, "Natural Gradient Works Efficiently in Learning," *Neural Computation*, vol. 10, no. 2, pp. 251–276, 1998.
- [45] R. Grosse and R. Salakhutdinov, "Scaling up Natural Gradient by Sparsely Factorizing the Inverse Fisher Matrix," in *ICML*, 2015, pp. 2304–2313.
- [46] N. N. Schraudolph, "Fast Curvature Matrix-Vector Products for Second-Order Gradient Descent," *Neural Computation*, vol. 14, no. 7, pp. 1723–1738, 2002.
- [47] A. C. Wilson, R. Roelofs, M. Stern, N. Srebro, and B. Recht, "The Marginal Value of Adaptive Gradient Methods in Machine Learning," *arXiv preprint arXiv:1705.08292*, 2017.
- [48] L. Bottou, F. E. Curtis, and J. Nocedal, "Optimization Methods for Large-Scale Machine Learning," *arXiv preprint arXiv:1606.04838*, 2016.
- [49] X. Glorot, A. Bordes, and Y. Bengio, "Deep Sparse Rectifier Neural Networks," in *AISTATS*, 2011, pp. 315–323.
- [50] K. He, X. Zhang, S. Ren, and J. Sun, "Delving Deep into Rectifiers: Surpassing Human-Level Performance on Imagenet Classification," in *ICCV*, 2015, pp. 1026–1034.
- [51] A. M. Saxe, J. L. McClelland, and S. Ganguli, "Exact Solutions to the Nonlinear Dynamics of Learning in Deep Linear Neural Networks," *ICLR*, 2014.
- [52] D. Mishkin and J. Matas, "All You Need is a Good Init," *ICLR*, 2016.
- [53] D. Sussillo and L. Abbott, "Random Walk Initialization for Training Very Deep Feedforward Networks," *arXiv preprint arXiv:1412.6558*, 2014.
- [54] S. S. Schoenholz, J. Gilmer, S. Ganguli, and J. Sohl-Dickstein, "Deep Information Propagation," *ICLR*, 2017.

- [55] A. Papoulis and S. U. Pillai, *Probability, Random Variables, and Stochastic Processes*. Tata McGraw-Hill Education, 2002.
- [56] R. M. Corless, G. H. Gonnet, D. E. Hare, D. J. Jeffrey, and D. E. Knuth, "On the LambertW Function," *Advances in Computational Mathematics*, vol. 5, no. 1, pp. 329–359, 1996.
- [57] Y. A. LeCun, L. Bottou, G. B. Orr, and K.-R. Müller, "Efficient Backprop," in *Neural Networks: Tricks of the Trade*. Springer, 2012, pp. 9–48.
- [58] R. Pascanu, T. Mikolov, and Y. Bengio, "On the Difficulty of Training Recurrent Neural Networks," in *ICML*, 2013, pp. 1310–1318.
- [59] P. Y. Simard, D. Steinkraus, J. C. Platt *et al.*, "Best Practices for Convolutional Neural Networks Applied to Visual Document Analysis." in *ICDAR*, 2003.
- [60] Y. LeCun, L. Bottou, Y. Bengio, and P. Haffner, "Gradient-Based Learning Applied to Document Recognition," *Proceedings of the IEEE*, vol. 86, no. 11, pp. 2278–2324, 1998.
- [61] N. Srivastava, G. E. Hinton, A. Krizhevsky, I. Sutskever, and R. Salakhutdinov, "Dropout: A Simple Way to Prevent Neural Networks from Overfitting," *JMLR*, vol. 15, no. 1, pp. 1929–1958, 2014.
- [62] D. C. Cireşan, U. Meier, L. M. Gambardella, and J. Schmidhuber, "Deep, Big, Simple Neural Nets for Handwritten Digit Recognition," *Neural Computation*, vol. 22, no. 12, pp. 3207–3220, 2010.
- [63] H. Jaeger and H. Haas, "Harnessing Nonlinearity: Predicting Chaotic Systems and Saving Energy in Wireless Communication," *Science*, vol. 304, no. 5667, pp. 78–80, 2004.
- [64] M. Lukoševičius and H. Jaeger, "Reservoir Computing Approaches to Recurrent Neural Network Training," *Computer Science Review*, vol. 3, no. 3, pp. 127–149, 2009.
- [65] J. Martens and I. Sutskever, "Learning Recurrent Neural Networks with Hessian-Free Optimization," in *ICML*, 2011, pp. 1033–1040.
- [66] M. Arjovsky, A. Shah, and Y. Bengio, "Unitary Evolution Recurrent Neural Networks," in *ICML*, 2016, pp. 1120–1128.
- [67] L. Jing, Y. Shen, T. Dubček, J. Peurifoy, S. Skirlo, M. Tegmark, and M. Soljačić, "Tunable Efficient Unitary Neural Networks (EUNN) and Their Application to RNNs," in *ICML*, 2017, pp. 1733–1741.
- [68] Z. Mhammedi, A. Hellicar, A. Rahman, and J. Bailey, "Efficient Orthogonal Parametrisation of Recurrent Neural Networks Using Householder Reflections," pp. 2401–2409, 2017.
- [69] S. Hochreiter and J. Schmidhuber, "Long Short-Term Memory," *Neural Computation*, vol. 9, no. 8, pp. 1735–1780, 1997.
- [70] M. P. Marcus, M. A. Marcinkiewicz, and B. Santorini, "Building a Large Annotated Corpus of English: The Penn Treebank," *Computational linguistics*, vol. 19, no. 2, pp. 313–330, 1993.
- [71] W. Zaremba, I. Sutskever, and O. Vinyals, "Recurrent Neural Network Regularization," *ICLR*, 2015.